HOW LUMPY IS THE MILKY WAY'S DARK MATTER HALO?

KATHRYN V. JOHNSTON,[1] DAVID N. SPERGEL,[2] AND CHRISTIAN HAYDN[1]

ABSTRACT

Cold dark matter (CDM) simulations predict that there are hundreds of lumps with masses greater than $10^7 \ M_\odot$ in the Milky Way halo. However, we know of only a dozen dwarf satellites close to this mass. Are these lumps simply lacking in stars, or is there a fundamental flaw in our most popular cosmology? By studying the tidal debris of known satellites, we can potentially address this question. In this paper, we quantify the effects of the dark matter lumps on tidal tails. The lumps scatter stars in the tidal tails from their original orbits, producing a distinctive signature. We simulate debris evolution in smooth and lumpy halo potentials, and use our simulations to motivate and test a statistical measure of the degree of scattering apparent in the angular position and radial velocity measurement of debris stars—the "scattering index." We find that the scattering index can in general distinguish between the levels of substructure predicted by CDM cosmologies and smooth Milky Way models, but the sensitivity of the debris depends on the orientation of the parent satellite's orbit relative to the largest lumps' orbits. We apply our results to the carbon star stream associated with the Sagittarius dwarf galaxy (Sgr), and find that these stars appear to be more scattered than we expect for debris orbiting in a smooth halo. However, the degree of scattering is entirely consistent with that expected because of the influence of the Large Magellanic Cloud, which is on an orbit that intersects Sgr's own. We conclude that the current data are unable to constrain CDM models. Nevertheless, our study suggests that future data sets of debris stars associated with other Milky Way satellites could provide strong constraints on CDM models.

Subject headings: dark matter — Galaxy: halo — Galaxy: kinematics and dynamics — Galaxy: structure

1. INTRODUCTION

Cold dark matter (CDM) models predict 2 orders of magnitude more dark matter halos than satellites observed around the Milky Way (Moore et al. 1999; Klypin et al. 1999). Solutions to this problem include self-interacting dark matter (Spergel & Steinhardt 2000), truncated power spectra (Kamionkowski & Liddle 2000), and the restriction of gas accretion to the lowest mass dark matter halos to be before the epoch of reionization (Bullock, Kravtsov, & Weinberg 2001). The first two solutions would get rid of the smallest dark matter halos entirely, while the latter would predict that only 1% of the satellite halos actually contain stars.

In this paper, rather than attempting to solve the problem, we discuss how we might tell observationally whether it is a problem in the first place. The satellite dark matter halos in the CDM models comprise about 10% of the total mass of the parent galaxy on roughly isotropic orbits distributed throughout the galaxy (Font et al. 2001). One idea is to look for signatures of these lumps around external galaxies in gravitationally lensed images of background quasars (Chiba 2002; Metcalf 2001; Metcalf & Zhao 2002). Similarly, Lewis et al. (2000) argue that if high-velocity H i clouds are associated with dark halos, then pixel gravitational lensing can detect such a halo in the form of massive compact objects. We also concentrate our study close to home. If such lumps truly exist around the Milky Way, then we would expect them to have some dynamical influence on the rest of the

visible Galaxy. For example, according to Lacey & Ostriker (1985), if the halo is entirely made of $10^6 \ M_\odot$ black holes, they would significantly heat our Galactic disk. Font et al. (2001) used numerical simulations to ask whether the coldness of our disk could be used in a similar fashion to limit the distribution of dark matter lumps seen in cosmological simulations that could be orbiting the Galaxy. Using one realization of lump masses and orbits taken from a ΛCDM model of a Galaxy-sized halo, they found that the heating caused by the lumps was less than the heating observed in the stellar populations in the disk, and concluded that the disk is not an efficient probe of this model.

Streams of debris from the destruction of Galactic satellites are another example of cold structures within the Milky Way that could be scattered by substructure in the potential. These streams tend to align along a single orbit (Johnston, Hernquist, & Bolte 1996; Johnston 1998; Helmi & White 1999) and hence would individually have lower cross section to interactions than the Galactic disk. Nevertheless, we chose to examine the response of these streams, rather than the disk, to perturbations for several reasons: (1) they will explore the outer regions of the Galactic potential that the disk does not experience; (2) we expect other sources of heating in this region (structures such as the bar, spiral arms, and giant molecular clouds in the disk) to be negligible; (3) if streams from several satellites could be studied, we have the potential of probing a larger portion of the Galaxy; and (4) these streams are often even colder than the disk itself and hence should be more sensitive to scattering.

We approach this problem of scattering numerically rather than analytically, because of both the nature of the predicted CDM mass distribution of lumps and the low cross sections of the streams. Scattering by the few most massive lumps in the distribution is expected to be most important, and the exact degree of scattering will depend on

[1] Van Vleck Observatory, Wesleyan University, Middletown, CT 06459; kvj@astro.welseyan.edu, ch@astro.wesleyan.edu.
[2] Princeton University Observatory, Princeton University, Princeton, NJ 08544; dns@astro.princeton.edu.

the relative orientation of the lump and debris orbits. Hence, the process is dominated by a few strong encounters rather than one that can be modeled, say, by integrating over many weak encounters in the impulsive regime. Nor would a simple analytic representation account for how the wake in the halo, excited by the most massive lumps, would affect the stream orbits. Weinberg's studies (Weinberg 1998b, 1995) of the affect of the Large Magellanic Cloud (LMC) on the disk of the Milky Way suggest that the inclusion of such a wake in the halo introduces a large enhancement to the expected response of the disk.

In § 2 we present our numerical approach to implementing the experiments described above. In § 3 we compare the evolution of tidal debris in smooth and lumpy potentials and propose an algorithm for distinguishing between the two with currently available data. In § 4 we apply our results to the stream of carbon stars known to be associated with Sgr. We summarize our conclusions and outline future prospects in § 5.

Note that during the final stages of preparation of this manuscript, two other papers have appeared on this subject (Mayer at al. 2001; Ibata et al. 2001a). We discuss their relation to our own work in § 5.

2. METHODS

2.1. *Particle Distributions*

We model our system with three sets of particles:

1. N_{halo} *smooth halo particles*.—These are equal mass and initially distributed as an equilibrium Hernquist (1990) model. This model is assumed to represent a $2.3 \times 10^{12}\ M_\odot$ halo, with scale length $a_{halo} = 30.6$ kpc, which was intended to mimic the Navarro-Frenk-White (NFW) profile (Navarro, Frenk, & White 1996, 1997) of a $v_{200} = 200$ km s^{-1} halo at $z = 0$ in a ΛCDM universe. These parameters were taken from Navarro & Steinmetz (2000). Since completion of the numerical portion of this project, the results of Navarro & Steinmetz (2000) have been withdrawn and the model we adopted has been shown to be too concentrated. Possible consequences of this are discussed below.

2. N_{lump} *lumps*.—These are each represented by rigid Hernquist (1990) models, with initial positions and velocities chosen at random from the same Hernquist (1990) distribution as above. Ghigna et al (1998) found that subhalo orbits in simulations of cluster formation are distributed isotropically but with an energy distribution that produces a density profile less concentrated than the parent halo. Since debris from Sgr orbits in and around a_{halo}, our simplification of adopting isotropic orbits with the same energy distribution as the smooth halo background will slightly overestimate the influence of the lumps, because the density of lumps toward the center of our halo is too high—an effect that will be compounded by the smooth halo itself being too concentrated.

The masses are chosen at random from a power-law distribution $dN/dm_{lump} \propto m_{lump}^{-5.75/3}$, whose form is taken from the endpoint of *N*-body cosmological simulations of CDM universes (Klypin et al. 1999; Moore et al. 1999). The upper and lower limits of the distribution are chosen so that 10% of the parent halo mass is contained in lumps with masses in the range 7×10^7–$2 \times 10^{10}\ M_\odot$, which approximately matches the level of substructure observed in *N*-body simulations (Moore et al. 1999). Moreover, Figures 4 and 5 in

Klypin et al. (1999) suggest that the degree of substructure in their ΛCDM model is similar to their CDM case; see also Font et al. (2001).

The scale lengths a_{lump} are set to $a_{lump} = 2r_s$, and the masses m_{lump} are chosen so that the potentials mimic "universal" Navarro et al. (1996) profiles to within 10% out to radii $10r_s$, with the mass dependence on concentration for a ΛCDM universe taken from Navarro & Steinmetz (2000). As noted above, the models we adopted have subsequently been shown to be too concentrated. This will again cause a slight overestimate of the efficiency of scattering.

Hernquist (1990) profiles rather than NFW profiles were used because of the saving in CPU time. We have not tidally truncated the models, but do not expect this to significantly affect our results.

Figure 1 summarizes the mass and scale distribution used in the simulations, with the solid lines representing the parameters for the Hernquist model and the dotted lines representing the parameters for the equivalent NFW model.

3. N_{test} *test particles*.—These are massless and are either distributed on circular orbits at $r = 0.5, 1.0, 2.0,$ and $4.0a_{halo}$ or on a range of orbits to mimic debris streams from Sgr. The initial conditions for the latter were generated by running a simulation of a satellite of $10^8\ M_\odot$ disrupting in a rigid representation of the halo potential described above (for simulation technique see Johnston et al. 1996) along an orbit similar to that expected for Sgr (see Ibata et al. 2001b). The times at which particles were lost from the satellite were noted. These times were then used to select initial conditions for 500 particles, starting from a point shortly after the pericentric passage at which they were first unbound.

2.2. *Force Computations*

The influence of the smooth halo particles on each other and on all other particles is calculated using a code that employs basis function expansions to represent the potential (Hernquist & Ostriker 1992) (we used the MPI version of the code, adapted from the original by S. Sigurdsson and B. Leary). This effectively smooths over all strong encounters (which we expect to be unimportant for this component), but does follow both large-scale collective fluctuations and the halo's response to disturbances by lumps.

The influence of the lumps on each other and on all other particles is calculated directly using the analytic form of the Hernquist (1990) potential.

The test particles respond to both the smooth halo and the lumps but do not otherwise interact. This simplification is valid for our application of tidal streams but would be a much poorer approximation were we trying to represent a system such as a disk, which has significant self-gravity.

2.3. *Integration*

Simple leap-frog integration was used throughout. The major computational expense arose from the large number ($N_{halo} \geq 10^7$) of smooth halo particles required (see § 2.5). However, since we were not interested in modeling strong encounters in this component in detail, we were able to use a large time step ($dt = 0.08$ in simulation units or about 4 Myr) for these particles, corresponding to 1/100 of the dynamical time at the half-mass radius of the parent galaxy. The lump and test particles were integrated with a much smaller time step $dt_{lil} = dt/2^{n_{lil}}$, where n_{lil} was chosen so the
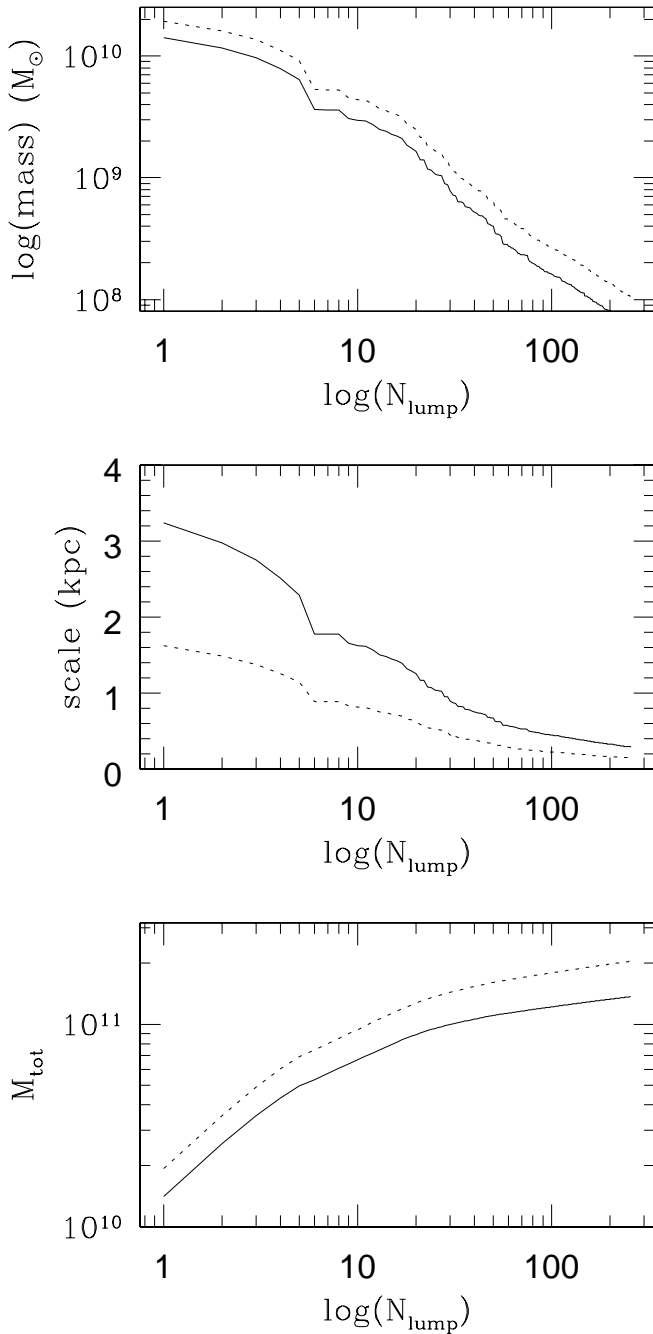
increase in computational cost for these integrations was not significant. For $N_{\mathrm{halo}} = 10^7$, $N_{\mathrm{lump}} = 20$, and $N_{\mathrm{test}} = 1000$, we could take $n_{\mathrm{lil}} = 8$ (or 256 small steps for every large step and $dt_{\mathrm{lil}} \sim 1.6 \times 10^4$ yr) with just a 20% increase in CPU time, and we double-checked our simulations by rerunning them with $n_{\mathrm{lil}} = 9$ to confirm convergence of the results. In general, we were looking to accurately follow encounters between features of a kpc with lumps traveling at 200 km s^{-1}, so we would expect $dt_{\mathrm{lil}} = (1 \text{ kpc}/200 \text{ km s}^{-1})/100 \sim 50{,}000$ yr to be a sufficiently small integration time step.

2.4. Initialization

The smooth halo distributions were allowed to run for 10 dynamical times to erase any effects from generating the initial conditions. For each set of lumps, the combined smooth halo and lumps were run for an additional 10 dynamical times as the lumps were grown slowly from zero to full strength to ensure no effects from suddenly introducing them. Finally, the output of the latter simulations were used as initial conditions in which the test particles were also run.

2.5. Required Particle Number, Number of Simulations, and CPU Cost

The finite number of halo particles will introduce potential fluctuations in addition to those due to the lumps (Weinberg 1993, 1998a), so we must ensure that the dominant cause of test-particle scattering is due to the lumps and not to numerical noise. To quantify the level of fluctuations in the halo due to the finite number of particles, we first ran models with $\log N_{\mathrm{halo}} = 4, 5, 6$, and 7 in isolation for 10 dynamical times and recorded the basis function expansion coefficients A_{nlm} calculated by the code during this time (where n refers to the radial basis function and lm refers to the spherical harmonic; see Hernquist & Ostriker 1992). The total potential energy can be written in terms of this expansion as $\Phi = \Sigma_{nlm} A_{nlm}^2$. Hence, the potential energy associated with each of the spherical harmonics is $\Phi_{lm} = \Sigma_n A_{nlm}^2$. The points in Figure 2 show the dispersion in the lowest order Φ_{lm} recorded during the isolated simulations. The dotted line shows the same measurement made in a simulation containing $N_{\mathrm{halo}} = 10^7$ particles and just one NFW lump. The plot suggests that to correctly model the influence of lumps on tidal streamers requires $N_{\mathrm{halo}} \sim 10^7$ particles, since otherwise scattering due to the finite resolution of the halo will compete with the effect being measured.

A second numerical consideration is that as long as the most massive particles have the greatest influence, the size of the effect we are trying to measure will depend on the exact choice of lump and streamer orbits. To gain a fair impression of the general evolution, it is necessary to run many simulations with different lump orbits.

The combined requirements of large particle number and multiple runs support our choice of running idealized simulations of fully formed galaxies over a restricted amount of time rather than trying to perform this experiment fully self-consistently in a cosmological context, which would add additional computational expense. Each simulation was first "relaxed" for 500 large steps and then followed for 1000 large time steps, or 10 dynamical times (corresponding to about 4 Gyr) for a total CPU cost of $\sim 225(N_{\mathrm{halo}}/10^7)$ hr. We ran more than 50 such simulations (a subset of which are presented here). To reduce this to manageable proportions (in memory and time), simulations were run on multiple nodes of the Wesleyan Beowulf-class supercomputer (WesWulf).

2.6. Parameter Sets

We present the results from a total of 37 simulations in this paper. Each simulation contained $N_{\mathrm{halo}} = 10^7$ halo particles and $N_{\mathrm{test}} = 4000$ test particles. The "control" simulation contained no halo lumps. The remaining 36 consisted of six sets of six random realizations of lump orbits for $N_{\mathrm{lump}} = 1, 4, 16, 64, 128$, and 256. Each set of simulations contained the same lump mass distribution, with increasing

numbers of lumps exploring further down the mass function. Since test particles were distributed on orthogonal orbits, our final results contained 12 different realizations of debris distributions, all starting from the same initial conditions but experiencing different time-dependent potentials.

3. RESULTS

3.1. Evolution of Orbits in Lumpy Potentials

As an example of evolution in a lumpy potential, Figure 3 plots the phase-space distribution of particles initially on circular orbits at $r = 0.5$ and 1.0 kpc at times $t = 0.8, 2.4,$ and 4 Gyr from one simulation containing $N_{lump} = 256$ lumps. The left-hand panels show positions in the orbital plane, while the right-hand panels show what observations we might make of the stars (assuming we could identify the initial orbital plane of the debris): angular distance $d\theta$ from the orbital plane and line-of-sight velocities v as a function of angle Ψ along the debris. The two things that are immediately apparent are (1) the orbital plane precesses over time (visible as a sinusoidal shape in the lowest $d\theta$ versus Ψ panel), and (2) particles initially distributed smoothly along the orbit become bunched in angular position and velocity.

Figures 4 and 5 repeat the above plots for the tidal debris particles in simulations with zero and $N_{lump} = 256$ lumps. Comparison of the right-hand panels of these plots clearly shows the orbital precession described above in the lumpy case. There is also some indication of additional structure along the orbit, but this is somewhat hidden by the intrinsic nonuniform distribution of debris along the orbit.

3.2. Interpreting Observations

From our qualitative assessment of Figures 3–5, we know we need to design a statistic that is sensitive to scattering in both angle and velocity along a debris stream rather than to large-scale effects such as overall heating. (Although precession is an additional effect, it is not observable since we do not in general know the original orbital plane of the satellite.) A natural choice is to look at Fourier series in the observed quantities,

$$B_{\Psi,m} = |\Sigma_k \, d\theta_k \exp^{im\Psi_k}| \,, \tag{1}$$

$$B_{v,m} = |\Sigma_k \, d\theta_k \exp^{imv_k/v_{max}}| \,. \tag{2}$$

In general, we expect the low-order B_m to contain signal that could be due to the periodic nature of debris orbits (in v) or debris density (in Ψ) along the orbit. However, higher B_m should be sensitive to scattering in the debris distribution.

To mimic how this might be applied to a real data set (such as Sgr), we (1) "observe" the Galactic latitude and longitude and line-of-sight velocity v of n debris particles in our simulations from a viewpoint 8 kpc from the Galactic center; (2) define the orbital plane to be the best-fit great circle to the angular data (Johnston et al. 1996); (3) find Ψ and $d\theta$ relative to this great circle; and (4) define a "scattering index" by summing over the Fourier expansion

$$B = \sqrt{\sum_{m=5,10} B_m^2} \,, \tag{3}$$
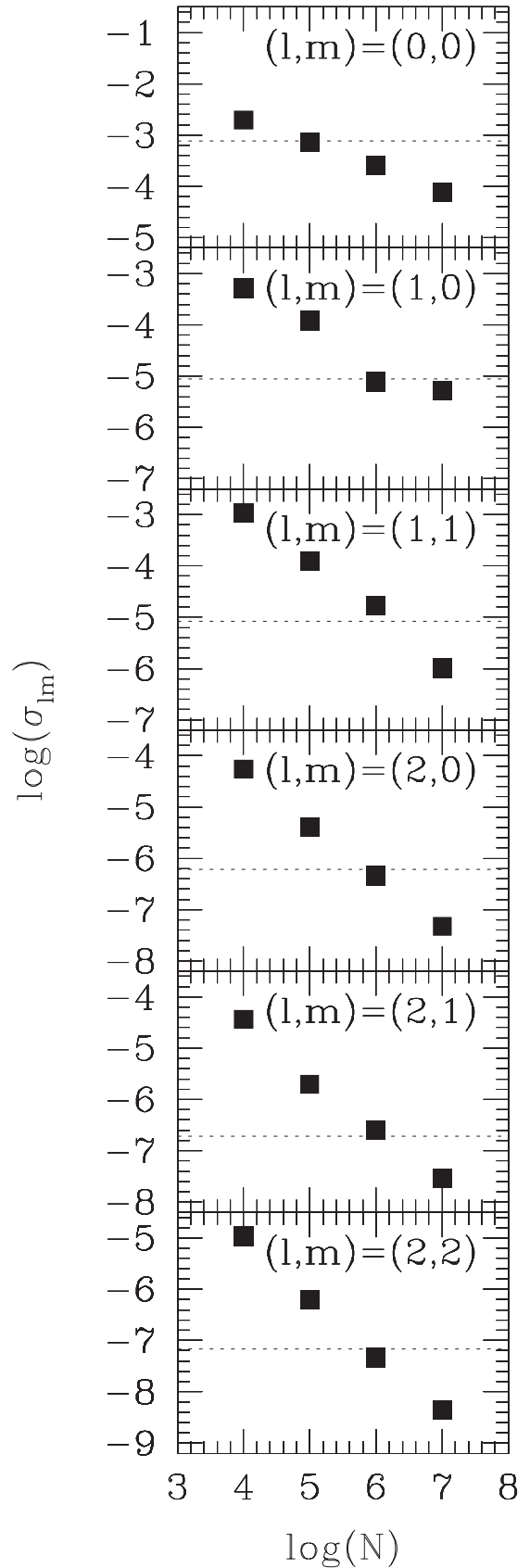
where

$$B_m^2 = B_{\Psi,m}^2 + B_{v,m}^2 \,. \tag{4}$$

FIG. 2.—Dispersion (calculated over 10 dynamical times) in the potential energy associated with each (l,m) spherical harmonic in a halo realized by N_{halo} particles. The dashed line shows the same calculation for a halo with $N = 10^7$ particles with the most massive CDM lump orbiting in it.
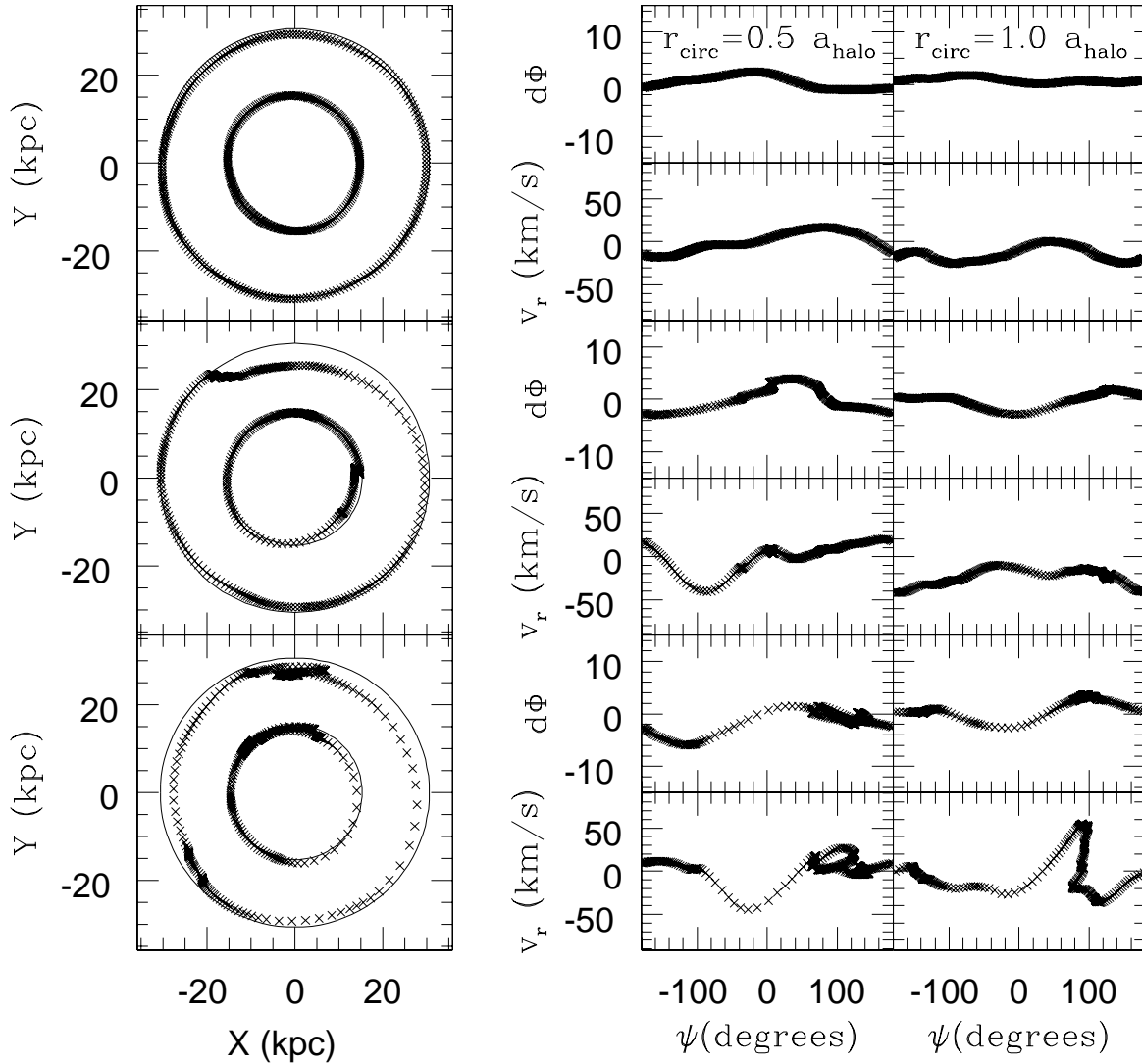
FIG. 3.—Final positions (*left*) and "observations" (*right*) of test particles initially on circular orbits after 1.3 (*top panels*), 2.6 (*middle panels*), and 4 (*bottom panels*) Gyr of evolution in a halo containing $N = 10^7$ particles and $N_{lump} = 256$ lumps.

Note that the lower limit in the summation was specifically chosen so that the statistic is not sensitive to large-scale effects such as intrinsic nonuniformity of tidal debris. From the mass and orbit of Sgr, we know that it takes a couple of orbits for debris to spread entirely along one "petal" (or radial oscillation) of a rosette orbit (Johnston 1998), and hence we would only expect a handful of distinct density enhancements due to dynamical effects at the turning point for debris lost during the last few Gyr. The upper limit was chosen to be much smaller than the number of debris particles analyzed in order to limit artificial enhancement of the statistic. Repeating our plots, varying both the upper and lower limits verified the intuition outlined above (i.e., the signal in the smooth halo simulation was stronger relative to the lumpy halo simulations for smaller lower and larger upper limits). The appropriate limits for a particular observed data set will depend on the number of debris members and suspected age of the debris.

The top panel of Figure 6 plots B_m against m calculated from all 500 of the debris particles from the $10^8 M_\odot$ satellite

at the end of the simulations, which each contained 256 lumps (*open squares and solid lines*), and contrasts these with the simulation containing no lumps *(closed squares and heavy lines)*. The bottom panel plots the scattering index for all the simulations as a function of number of lumps (*open squares*), with the heavy line showing B for the no-lumps case. In general, we find that we expect to be able to use this index to distinguish between sΛCDM and nonlumpy Milky Way halos roughly 90% of the time. There is a tendency for the majority of the scattering to be caused by the very largest lumps (i.e., no perceptible trend in the mean amplitude of B for $N_{lump} > 10$). However, the large variance in the results for a given N_{lump} emphasizes that the degree of scattering is very sensitive to the relative orientation of lump and debris orbits. In some cases, all scattering could clearly be attributed to the most massive or few most massive lumps, while in others there was a significant increase in B between the $N_{lump} = 4$ and 16 simulations. In the case of the Milky Way, the existence of the LMC and SMC means that the number of very massive lumps orbiting the Milky Way is in rough
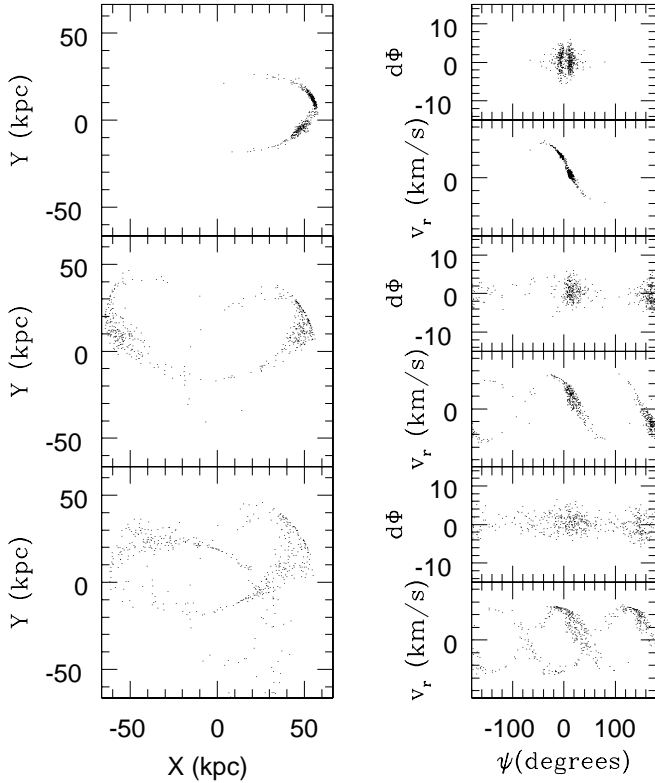
FIG. 4.—Final positions (*left*) and " observations " (*right*) of test particles initially on Sgr debris orbits after 1.3 (*top panels*), 2.6 (*middle panels*), and 4 (*bottom panels*) Gyr of evolution in a halo containing $N = 10^7$ particles and $N_{lump} = 0$ lumps.
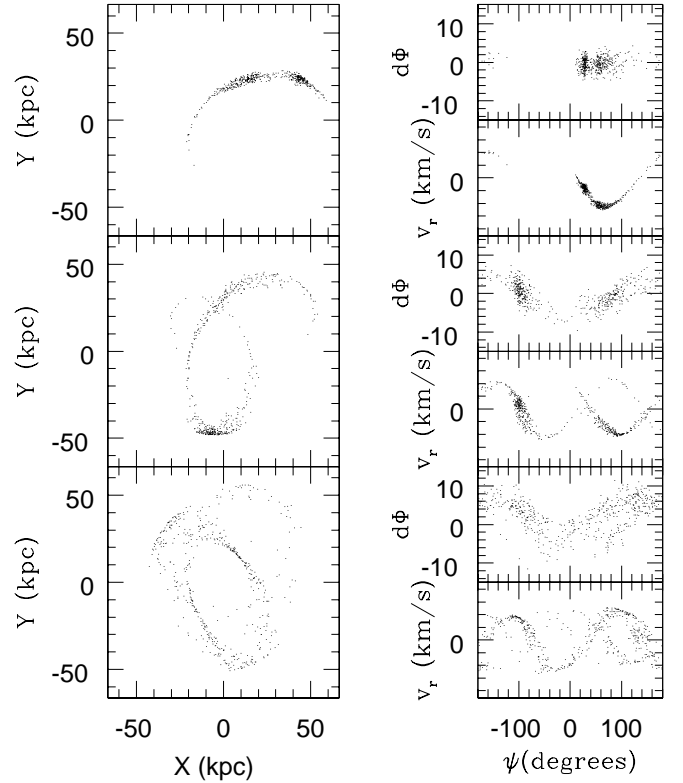
FIG. 5.—Final positions (*left*) and " observations " (*right*) of test particles initially on Sgr debris orbits after 1.3 (*top panels*), 2.6 (*middle panels*), and 4 (*bottom panels*) Gyr of evolution in a halo containing $N = 10^7$ particles and $N_{lump} = 256$ lumps.

agreement with the cosmological simulations. Hence, for a clear test of sΛCDM we need to find debris on orbits that are not heavily influenced by these objects.

4. APPLICATION TO OBSERVATIONS: SGR'S CARBON STAR STREAM

Ibata et al. (2001b) report the discovery of a set of carbon stars that closely align with the great circle defined by Sgr's position and proper motion. They find that this stream is too thin to be easily explained in models of the Galaxy that have oblate halos because debris orbits in nonspherical potentials precess beyond the width of the stream within the typical lifetimes of the carbon stars (47 of the 104 stars lie within $10°$ of Sgr's great circle, which intercepts less than one-quarter of the total survey area). Such a cold stream provides an obvious testing ground for models that predict dark matter substructure around the Milky Way.

Carbon stars have ages ranging from a few to 6 or 7 Gyr. Hence, we expect the length of our simulations (4 Gyr) to be a fair representation of how long this debris may have been orbiting independently.

Figure 7 repeats Figure 6 but for 47 tidal debris particles chosen at random at the end of the simulations. In this case, the particles were again viewed at a point 8 kpc from the Galactic center chosen slightly out of the orbital plane of the satellite to reflect the Sun's orientation relative to Sgr's own orbit. To mimic the real survey, we also restricted our simulated survey to only those particles farther than $30°$ from the Galactic disk and within $10°$ of the best-fit great

circle of the full debris distribution. In the top panel of Figure 7, the points and lines represent the results from just one set of particles in each simulation that contained $N_{lump} = 256$. In the bottom panel, the points represent the results for one set of 47 particles chosen from each simulation. The lower shaded region in the bottom panel shows dispersion around the average of the results for 10 different particle sets in the no-lumps case. The heavy dashed line in both panels is the result of the identical analysis performed on the Sgr carbon star data set. The figure suggests that the Sgr carbon star set exhibits a level of substructure inconsistent with debris orbits on a smooth, spherical potential.

The " lumps " that we are already aware of in the Milky Way's halo consist of the LMC, SMC, and the eight other dwarf spheroidal satellites. Since our results clearly depend on the exact orientation of the orbits of the largest lumps' masses relative to the debris orbits, we ran one final simulation in which we integrated the Sgr debris in a halo containing a satellite of mass $10^{10} M_{\odot}$ in an orbit like that of the LMC (roughly perpendicular to Sgr's orbit with a pericenter comparable to Sgr's apocenter). The results of the application of the scattering index to the output from the simulation are shown as heavy dotted lines in Figures 6 and 7. We conclude that for the current Sgr data set, the degree of scattering is entirely consistent with debris perturbed by the LMC alone. Moreover, Figure 6 implies that even with a larger data set associated with Sgr, it will be difficult to distinguish between a sΛCDM halo and a smooth one. Although disappointing, this result might have been anticipated from previous studies that have found plausible sce-
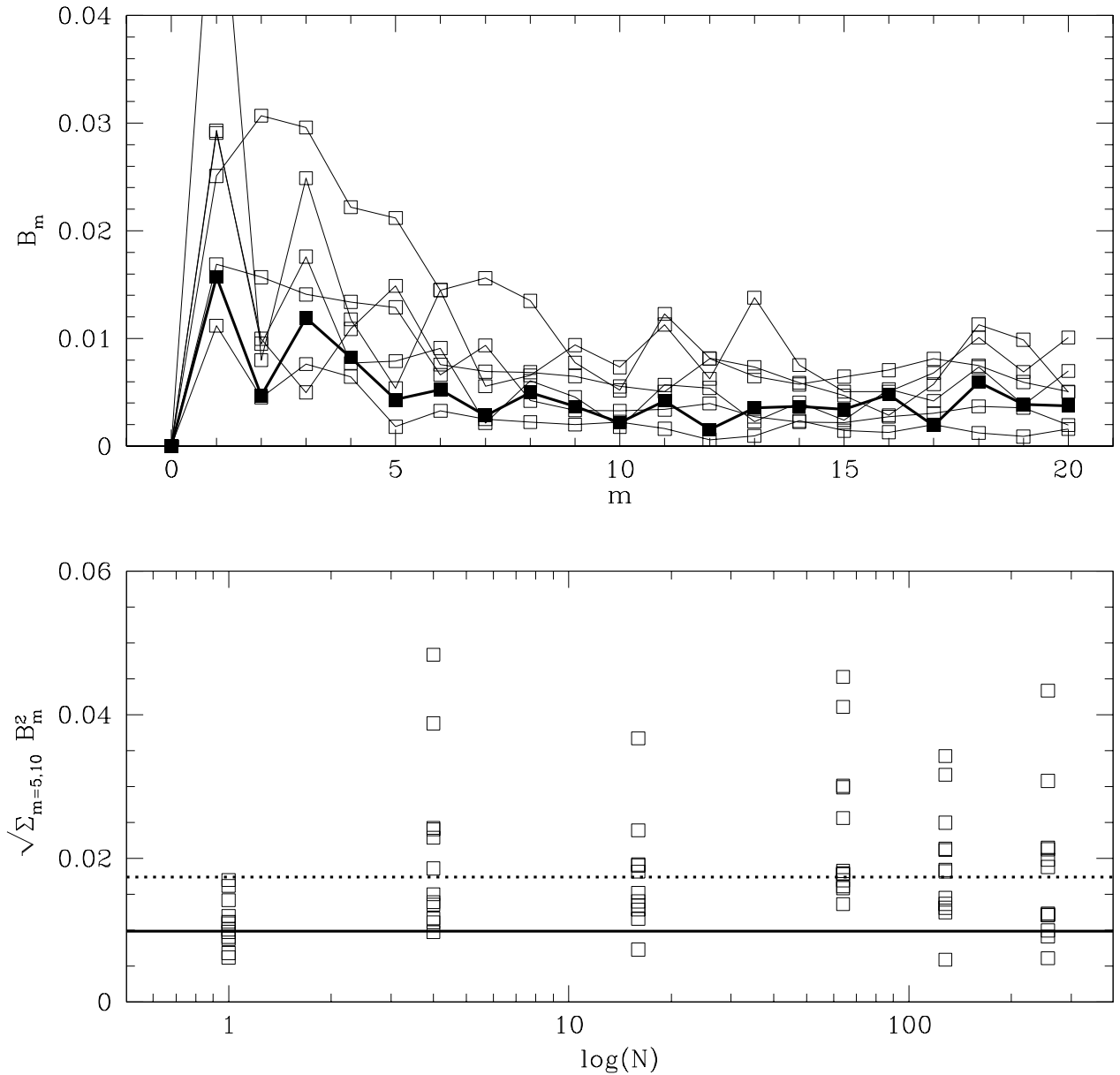
FIG. 6.—*Top*: Components of the scattering index B_m, calculated from the final observations of 500 Sgr debris particles, plotted as a function of Fourier number m (see eq. [4] for definition). Open squares and solid lines show results for all realizations of halos with $N_{lump} = 256$ lumps on random orbits. Filled squares and heavy lines show the result for evolution in a smooth halo. *Bottom*: The scattering index B (see eq. [3]) calculated for all 500 debris particles at the end of each simulation, as a function of the number lumps in the simulation. The heavy line indicates B for a simulation containing no lumps, and the dotted line is for one containing a single lump of mass $10^{10} M_\odot$ on an LMC-like orbit.

narios of strong interactions between the LMC and Sgr (Zhao 1998).

5. CONCLUSIONS AND FUTURE PROSPECTS

In this paper, we show that it is possible to distinguish between smooth and lumpy Milky Way halos by quantifying the coldness of tidal streams. We propose a " scattering index," based on position and radial-velocity measurements of stars, that is sensitive to small-scale perturbations in the debris rather than large-scale effects such as variations in debris density or line-of-sight velocity (because of its basic dynamical properties). We found that this statistic, when applied to measurements of 500 stars in a single debris trail, could distinguish between smooth, spherical Milky Way

models and those containing a level of substructure consistent with sΛCDM models 90% of the time. Most scattering was due to the few largest lumps, and the degree of scattering was very sensitive to the exact orientation of lump and debris orbits.

These results agree qualitatively with those of Mayer et al. (2001) and Ibata et al. (2001a). Mayer et al. (2001) present images from simulations of tidal tails evolved in fully self-consistent sΛCDM models to illustrate to what extent the tails are disrupted. This approach has the advantage of being able to follow the evolution of debris within a cosmological context, but, as noted in § 2.5, is limited by the resolution and cost of such simulations to single realizations of galaxies that may not be adequately resolved to conquer intrinsic scattering due to numerical noise. Ibata et al.
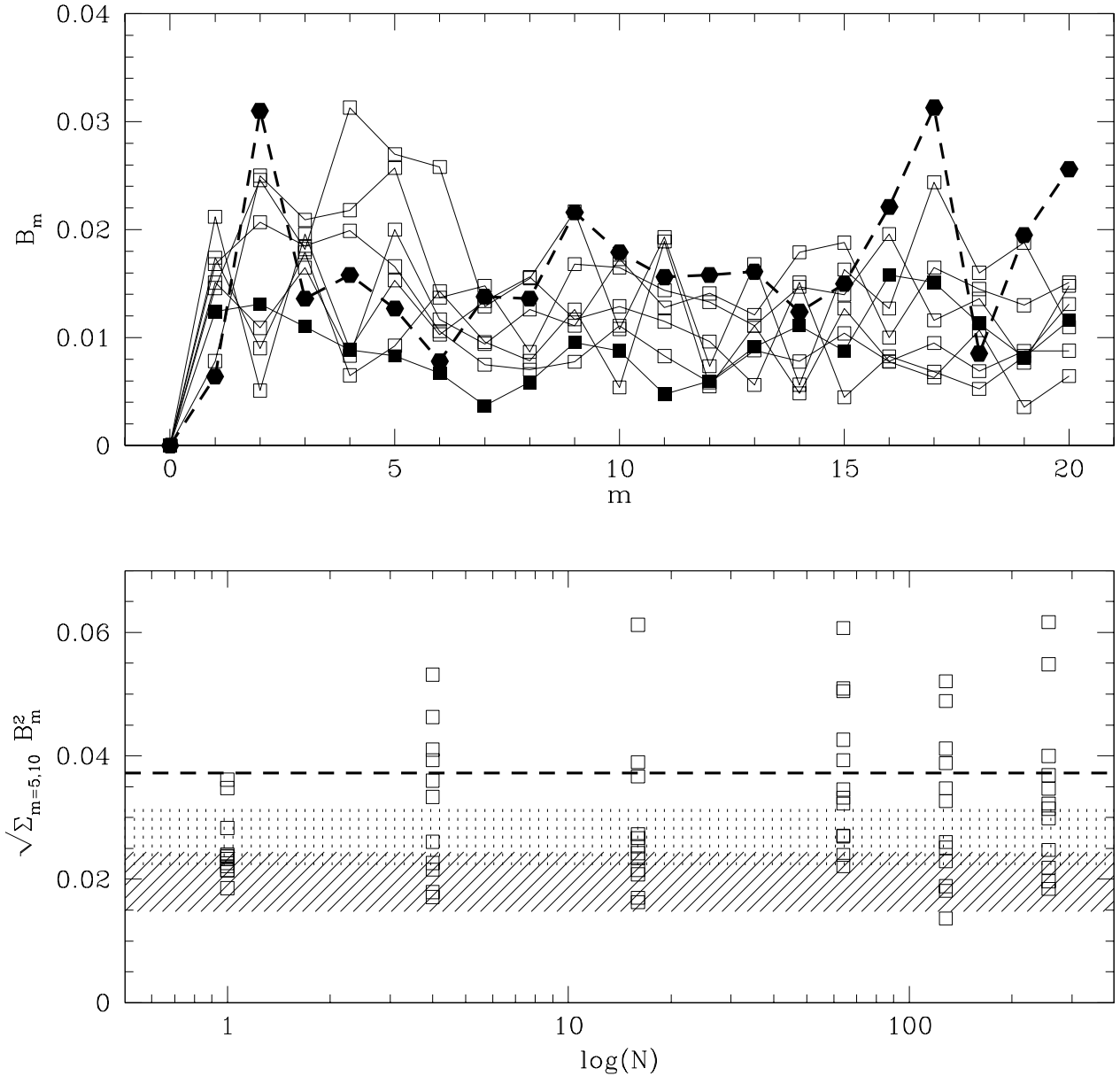
Fig. 7.—Same as Fig. 6, but for 47 particles selected to be within $10°$ of the best-fit great circle to the debris particles at the end of the simulation, and at Galactic latitudes $|b| > 30°$. The heavy dashed lines in both panels show the result of applying the same statistic to the 47 carbon stars found within $10°$ of Sgr's orbital plane. In the bottom panel, the lower shaded region indicates the dispersion around the mean for 10 sets of 47 randomly selected particles from the simulation containing no lumps. The upper shaded region shows the same region for a simulation containing just one lump, mass $10^{10} M_\odot$ on an LMC-like orbit.

(2001b) simplify our own approach by modeling only the influence of lumps on the debris, not accounting for the halo wake in their simulations and hence (as they note) underestimating the true magnitude of the lump influence. Nevertheless, they demonstrate that scattering due to dark matter lumps should be easily detectable in the angular momentum distribution of debris from globular clusters—an experiment that will become feasible with the launch of the *Global Astrometric Interferometer for Astrophysics* (*GAIA*) satellite in the second decade of the 21st century.

In contrast to Ibata et al. (2001a), our own aim was to look at the feasibility of constraining the halo dark matter distribution with data available today or in the near future. Following this aim, we applied our scattering index to the carbon star stream associated with Sgr and found that it contains more scattering than would be expected if it were

orbiting in a smooth Milky Way. We then demonstrated that the level of scattering in Sgr's debris is entirely consistent with perturbations by the LMC alone. We conclude from our study that the current data are unable to place limits on the level of dark matter substructure in the Milky Way's halo. Moreover, the specific alignments of the LMC's and Sgr's orbits mean that a larger sample of Sgr's debris is unlikely to improve the sensitivity of our statistic.

Three other factors could be responsible for the large B measured for the Sgr sample: we have not taken into account the contamination of the carbon star sample by non-Sgr stars; we have assumed that the Galaxy is perfectly spherical and that the stream is not broadened by precession of the debris orbits; and we have modeled the Galaxy's potential as nonevolving (other than in response to the lumps) over the lifetime of the stream. Despite these limita-

tions, we remain optimistic about the use of tidal debris to constrain dark matter substructure in the future. The first problem should be solved once we have a large enough data set to identify Sgr debris by continuous velocity variations across the sky, and the second could be addressed with such a clean sample by looking for anomalous local scatterings in velocity. The importance of the last problem is rather harder to assess, since it will depend on the accretion history of the Milky Way. In popular dark matter scenarios, a Milky Way–mass dark halo is likely to have roughly doubled its mass in the last 4 Gyr (J. Bullock 2001, private communication). However, the coldness and age of the Milky Way's thin disk suggest that it has not undergone a major merger during that time, and if this mass were instead accreted gradually, we would expect debris streams to maintain their coherence (Zhao et al. 1999). These ideas should be tested more thoroughly with fully self-consistent cosmological simulations, but the current resolution of these simulations prohibits a clear separation of numerical and physical scattering of debris particles at the level of interest (as noted in § 2.5).

Nor are we limited to considering only tidal streamers from Sgr. There is mounting evidence to suggest that many of the Milky Way's other satellites (and globular clusters) have associated debris (Grillmair et al. 1995; Irwin & Hatzidimitriou 1995; Majewski et al. 2000b). This evidence is currently limited to overdensities of material close to these objects and hence too young dynamically to be of use for our study. However, several deep-halo surveys are currently underway that have the potential of tracing these streams out further (Ivezić et al. 2000; Yanny et al. 2000; Majewski et al. 2000a; Morrison et al. 2000). If extensive debris is found, then these satellites, all of which have lower masses than Sgr, would provide even colder streams, which should be even more sensitive probes of substructure. They are also on different orbits, exploring other regions of the halo where the LMC's influence will be less dominant. In particular, tails from the most distant dSph—e.g., Leo I, Leo II, Fornax, and Carina—may be less likely to be influenced by the LMC, although this can only be more realistically assessed with accurate measurements of their proper motion and estimates for their orbits. In contrast, the alignment of Ursa Minor and Draco's proper-motion vectors with the "Magellanic Plane"—coinciding with the LMC, SMC, and Magellanic Stream (Kunkel & Demers 1976; Lynden-Bell 1982; Lynden-Bell & Lynden-Bell 1995; Palma, Majewski, & Johnston 2002)—suggests that debris from these satellites may be more significantly disturbed by the LMC.

Looking even further into the future, astrometric satellite programs such as NASA's *Space Interferometry Mission* (*SIM*) and ESA's *GAIA* will provide the two additional dimensions of proper motion to allow a more rigorous measure of scattering to be defined, such as that proposed by Ibata et al. (2001a).

REFERENCES

Bullock, J. S., Kravtsov, A. K., & Weinberg, D. H. 2001, ApJ, 548, 33
Chiba, M. 2002, ApJ, 565, 17
Font, A. S., Navarro, J. F., Stadel, J., & Quinn, T. 2001, ApJ, 563, L1
Ghigna, S., Moore, B., Governato, F., Lake, G., Quinn, T., & Stadel, J. 1998, MNRAS, 300, 146
Grillmair, C. J., Freeman, K. C., Irwin, M., & Quinn, P. J. 1995, AJ, 109, 2553
Helmi, A., & White, S. D. M. 1999, MNRAS, 307, 495
Hernquist, L. 1990, ApJ, 356, 359
Hernquist, L., & Ostriker, J. P. 1992, ApJ, 386, 375
Ibata, R. A., Lewis, G. F., & Irwin, M. J. 2001a, MNRAS, submitted (astro-ph/0110690)
Ibata, R. A., Lewis, G. F., Irwin, M. J., Totten, E., & Quinn, T. 2001b, ApJ, 551, 294
Irwin, M., & Hatzidimitriou, D. 1995, MNRAS, 277, 1354
Ivezić, Z., et al. 2000, AJ, 120, 963
Johnston, K. V. 1998, ApJ, 495, 297
Johnston, K. V., Hernquist, L., & Bolte, M. 1996, ApJ, 465, 278
Kamionkowski, M., & Liddle, A. R. 2000, Phys. Rev. Lett., 84, 4525
Klypin, A. A., Kratsov, A. V., Valenzuela, O., & Prada, F. 1999, ApJ, 522, 82
Kunkel, W. E., & Demers, S. 1976, R. Greenwich Obs. Bull., 182, 241
Lacey, C. G., & Ostriker, J. P. 1985, ApJ, 299, 633
Lewis, G. F., Bland-Hawthorn, J., Gibson, B. K., & Putman, M. E. 2000, PASP, 112, 1300
Lynden-Bell, D. 1982, Observatory, 102, 202

Lynden-Bell, D., & Lynden-Bell, R. M. 1995, MNRAS, 275, 429
Majewski, S. R., Ostheimer, J. C., Kunkel, W. E., & Patterson, R. J. 2000, AJ, 120, 2550
Majewski, S. R., Ostheimer, J. C., Patterson, R. J., Kunkel, W. E., Johnston, K. V., & Geisler, D. 2000, AJ, 119, 760
Mayer, L., Moore, B., Quinn, T., Governato, F., & Stadel, J. 2001, MNRAS, submitted (astro-ph/0110386)
Metcalf, R. B. 2001, preprint (astro-ph/0109347)
Metcalf, R. B., & Zhao, H. S. 2002, ApJ, 567, L5
Moore, B., Ghigna, S., Governato, F., Lake, G., Quinn, T., Stadel, J., & Tozzi, P. 1999, ApJ, 524, L19
Morrison, H. L., et al. 2000, AJ, 119, 2254
Navarro, J. F., Frenk, C. S., & White, S. D. M. 1996, ApJ, 462, 563
———. 1997, ApJ, 490, 493
Navarro, J. F., & Steinmetz, M. 2000, ApJ, 528, 607
Palma, C., Majewski, S. R., & Johnston, K. V. 2002, ApJ, 564, 736
Spergel, D. N., & Steinhardt, P. J. 2000, Phys. Rev. Lett., 84, 3760
Weinberg, M. D. 1993, ApJ, 410, 543
———. 1995, ApJ, 455, L31
———. 1998a, MNRAS, 297, 101
———. 1998b, MNRAS, 299, 499
Yanny, B., et al. 2000, ApJ, 540, 825
Zhao, H. 1998, ApJ, 500, L149
Zhao, H., Johnston, K. V., Hernquist, L., & Spergel, D. N. 1999, A&A, 348, L49